Laser Ablation of Optical Glasses in the Linear and Non-Linear Absorption Regime Using Ultrashort Pulsed Laser Radiation from Deep UV to IR

Astrid Sassmannshausen*, Martin Kratz, Florian Withake, and Daniil Podkatilov

Fraunhofer Institute for Laser Technology (ILT), Aachen, Germany
**Corresponding author's e-mail: astrid.sassmannshausen@ilt.fraunhofer.de*

An alternative approach to conventional fabrication methods for optical components is the laser-based process chain. In that case, precise form generation can be achieved using ultrashort pulse (USP) laser ablation. Precise control of the ablation depth and surface roughness is a crucial requirement for optical applications. Current developments in USP laser beam sources lead to an increase in output power, enabling high harmonic generation with sufficient pulse energy for the ablation of glass materials. Optical glasses, depending on their specific chemical composition, show a drop in transparency in the UV-range. In this paper, the influence of the pulse duration, exemplary for 200 fs and 8 ps, on the ablation behavior of the optical glasses N-BK7 and P-SF69 is investigated comparing an IR-wavelength of 1030 nm to deep-UV-wavelengths of 257-266 nm. In contrast to IR-ablation, where the ps-pulse duration results in a more efficient ablation compared to fs-pulses, the ablation efficiency of N-BK7 is independent of the pulse duration in DUV. Furthermore, the surface roughness can be reduced to Sa < 0.14 µm using DUV laser radiation. The ablation behavior of P-SF69 is melt-dominated, resulting in a smooth roughness down to Sa = 45 nm, near to optical quality.
DOI: 10.2961/jlmn.2026.01.2008
Keywords: ultrashort pulse, glass ablation, optical glass, deep-UV, femtosecond, picosecond, ablation efficiency, surface roughness, N-BK7, P-SF69

1. Introduction

The optical components market is currently pushed by an increasing demand for miniaturization, shortened production times, digitalization and high durability of the optical elements. Therefore, innovative optical system designs increasingly contain micro-optical components, aspheric lenses and free-form surfaces. Applications are, e.g., imaging systems, endoscope optics, achromats and sensor technology. Such complex shaped geometries, especially when differing from a rotationally symmetric shape, are difficult to manufacture with conventional fabrication methods like mechanical milling, grinding and polishing. One upcoming alternative process technology currently in development for glass optical elements is offered by a laser-based process chain. Precise form generation can be achieved by ultrashort pulse (USP) laser ablation, resulting in a surface roughness of typically $\boldsymbol{Sa}$ = 0.4-1 µm [1–4] using IR-laser radiation (mostly about 1030-1064 nm). The fabrication of different micro-optical devices from fused silica by USP laser ablation at 1030 nm wavelength has been presented, including axicons [5], spherical and cylindrical micro-lenses [1,6]. As the surface roughness after ablation does not fulfill optical requirements, subsequent CO_2-laser polishing can be conducted for further reduction of the surface roughness [1,5–8].

Laser ablation of glass is still a challenging task when it comes to precise micro processing. The ablation behavior, determining the achievable precision of ablation, is dependent on material properties like absorptivity, absorption depth, and thermal conduction. Due to the high absorption in the MIR-range, glass ablation can be performed with CO_2-laser radiation [7,9–11]. The second area, where glasses are typically highly absorptive, is the range of deep-UV-(DUV) wavelengths, which is addressed by studies on nanosecond excimer laser ablation, e.g. at 193, 248 and 308 nm wavelength [12,13]. Both approaches, using ns-µs or continuous wave (cw) laser radiation, are influenced by pronounced heat affected zones (HAZ) diminishing the ablation quality.

In contrast to longer pulse durations and cw-radiation, USP laser radiation is beneficial for precise material ablation and well-known for high quality machining. The reduction of melt formation and HAZ when using fs-ps pulses compared to longer pulse durations is based on the very short duration of the laser-material interaction. Absorption in transparent materials of standard solid-state laser wavelengths in the infrared-range is enabled by the high intensity of the USP laser pulses ($I > 10^{12}$ W/cm^2) triggering non-linear absorption mechanisms [14]. Interaction and absorption mechanisms of dielectric materials with USP laser radiation have been investigated fundamentally. The excitation of electrons from the valence into the conduction band is initiated by non-linear multi-photon absorption, that can be accompanied by tunnel ionization [15,16]. Further linear absorption of photons takes place by Inverse Bremsstrahlung absorption, impact and Avalanche ionization [15,17,18]. Due to the time scale of the sequence of different ionization processes, the overall ionization can be dominated by single ionization mechanisms depending on pulse duration and intensity. With increase of the pulse duration from fs to ps and with increasing intensity, the dominating mechanism is

shifted from multi-photon ionization to Avalanche ionization [19].

USP ablation of transparent materials using VIS-IR laser radiation is widely investigated. Due to the high intensities required for absorption, the process is susceptible to cracking and formation of a certain heat-affected zone. Current developments in USP laser beam sources lead to increasing output powers enabling high harmonic generation with sufficient pulse energy for the ablation of dielectric materials. DUV modules for fourth harmonic generation of solid-state USP laser beam sources became commercially available in the last few years. Thus, research on laser material processing with DUV USP laser radiation is currently growing. Single pulse, line and small area processing of ultra-thin display glass was studied using a 257 nm 500 fs laser [20]. Compared to processing results achieved with 350 fs at 515 nm, this study shows a reduction of crack-formation, roughness and chipping with the DUV setting [20]. Single pulse and line ablation behavior of BK7 and soda-lime glass with a 300 fs, 206 nm laser is investigated by another recent publication [21]. The researchers state a primarily photomechanical ablation mechanism and a reduced penetration depth of the DUV pulses compared to longer wavelengths as an explanation for a low surface roughness after ablation with 206 nm [21]. The DUV ablation behavior in dependence on the number of pulses is investigated for soda-lime glass with 206 nm at 300 fs, regarding width, efficiency and surface roughness of single spot ablation. A controllable precision in depth ranging from nm-µm is presented and high-quality ablation with low HAZ is related to linear light absorption. [22] As glass ablation with IR-wavelengths is already under investigation for a longer time, more extensive research is available including three-dimensional ablation processes, analysis of process efficiencies and the influence of various parameters [23–25]. In contrast, mostly single spot, single line and small area processing regarding one laser setup is investigated for DUV ablation.

In this paper, the ablation behavior of the two optical glasses borosilicate-crown N-BK7 and dense-flint P-SF69, that represent two different types of optical glasses, is presented. Results obtained with USP-DUV-laser radiation are compared to USP-IR-laser radiation for use in the fabrication of optical components. The influence of the pulse duration on the ablation behavior in terms of ablation quality and ablation efficiency is investigated for both wavelengths. Therefore, pulse durations of 200 fs and 8 ps are applied for both, IR laser radiation at 1030 nm and DUV laser radiation at 257-266 nm.

2. Methods and materials

2.1 Materials

Optical glasses are specified by mainly the two characteristic properties refractive index and dispersion, which can be given by the Abbe number. In this paper, two glass materials, each from a different type of optical glasses, are used for the ablation study. SCHOTT N-BK7® is used, representing borosilicate-crown glasses, that are characterized by a relatively low refractive index and low dispersion, i.e. high Abbe number. The second glass is the dense-flint glass SCHOTT P-SF69 exhibiting a larger refractive index and a higher dispersion. The material properties are given in **Table 1** by means of the refractive index and Abbe number.

Table 1 Refractive index and Abbe number of the optical glasses N-BK7 and P-SF69 [26].

Glass material	Refractive index [-]	Abbe number [-]
N-BK7	1.52	64.17
P-SF69	1.72	29.23

The transmission spectra of N-BK7 and P-SF69 show the typical high transparency in the VIS-NIR range and a drop of the transparency at UV-wavelengths. The transmittance, measured at 10 mm sample thickness [26], for both glasses is given in **Fig 1**.

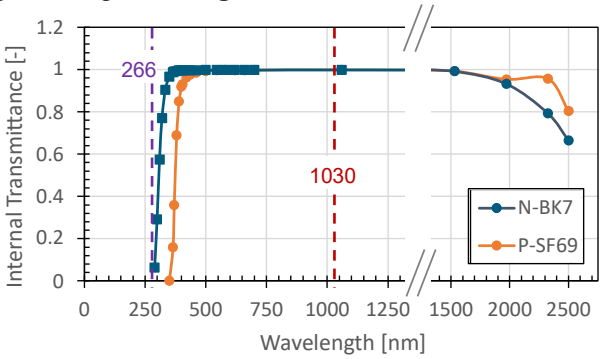

Fig 1 Internal transmission of SCHOTT N-BK7 ® and SCHOTT P-SF69, measured at 10 mm sample thickness [26].

The transmittance for the wavelength of 1030 nm is around 0.999 for N-BK7 and P-SF69. The drop of the transmittance in the (deep-)UV range is shifted to higher wavelengths for P-SF69 compared to N-BK7. The transmittance of a 10 mm tick P-SF69-sample reaches $T = 0$ at 350 nm, N-BK7 reaches $T = 0.063$ at 290 nm wavelength for a sample thickness of 10 mm. [26] The thicknesses of the polished samples used for the ablation study are d_1 = 8 mm for N-BK7 and d_2 = 5 mm for P-SF69.

2.2 Experimental setup

The influence of the pulse duration, exemplary for the pulse durations $\tau_{P,1}$ = 200 fs and $\tau_{P,2}$ = 8 ps, is investigated in the DUV range λ_1 = 257-266 nm compared to the IR-wavelengths λ_2 = 1030-1064 nm. Therefore, three different laser systems are used in the study. All laser beam sources used emit linearly polarized laser radiation.

The experimental setup for the IR-experiments consists of a tunable USP laser beam source (Carbide, Light Conversion) with a wavelength of 1030 nm and the pulse durations 200 fs and 8 ps are used. Pulses are generated by chirped pulse compression. Repetition rates of 10-100 kHz are used during the test series. Two-dimensional processing is performed with a galvanometer scanner (intelliSCAN de 14, SCANLAB). The laser beam is focused on the sample surface by a f-theta-lens with focal length f_1 = 80 mm, resulting in a focal diameter (1/e²) of $2w_{0,1}$ = 25 µm. The focal diameter was measured with a CCD camera and was additional calculated using the Liu-method [27].

For the DUV fs-experiments, the laser radiation from a USP laser beam source of 1030 nm (Carbide, Light Conversion) is converted to 257 nm by a fourth harmonic module. The final pulse duration is about 200 fs. Two-dimensional

processing is achieved by a linear x-y-stage. The repetition rate is constant at 10 kHz for the DUV-fs test series. Focusing is achieved with an aspheric lens with focal length of f_2 = 50 mm resulting in a focal diameter (1/e²) of $2w_{0,2}$ = 10.9 µm (calculated with the Liu-method [27]).

DUV ps-experiments are conducted with a fourth harmonic USP laser beam source (HyperRapid NXT 266, Coherent) emitting at 266 nm, resulting from the conversion of 1064 nm. The pulse duration of the laser is transform-limited to 8 ps and the repetition rate used is 10 kHz. The system is equipped with a galvanometer scanner (excelliSCAN 14, SCANLAB) for two-dimensional beam deflection. The focal diameter (1/e²) after focusing by a f-theta-lens with focal length f_3 = 103 mm is calculated to $2w_{0,3}$ = 11.5 µm by applying the Lui-method [27].

2.3 Processing strategy

Process characteristics, including ablation efficiency (ablation rate per average power [mm³/min/W]), ablation depth and surface roughness, are obtained by ablation of several square cavities on the glass substrates. The cavities with an edge length between 0.5 and 1.5 mm are ablated by overlapping linear scanning lines with pulse and line overlap of 60 %. The pulse and the line overlap are calculated based on the 1/e² focal spot diameter. The direction of the scanning lines is rotated by an angle of 90° between successive layers. In this paper, the term layer refers to a single scan pass of the ablated area. The cavities are ablated with N = 5-10 layers, which is specified in detail in the relevant sections. The influence of the number of layers and the comparability of results are analyzed and discussed in **section 3.1**.

The ablation depth and the ablation roughness are measured with a laser scanning microscope (LSM) (VK-X3000, Keyence), that is equipped with 404 nm emitting semiconductor laser as measuring light source. A 50x objective, which exhibits a lateral resolution of 0.264 µm, is used for the roughness measurements. The three-dimensional surface roughness Sa is evaluated according to ISO 25178.

In the second part of this study, we utilize a repetition rate of 10 kHz to isolate the effects of wavelength, pulse duration, pulse overlap, and track distance from accumulative phenomena such as heat accumulation, plasma shielding, and particle shielding. This approach allows us to focus on the fundamental mechanisms underlying the interactions during laser ablation. However, for the transfer of these findings to industrial applications, it is essential to increase the repetition rate to ≥100 kHz, where the aforementioned accumulative effects become more pronounced and must be taken into account.

3. Results and discussion

3.1 Influence of the number of layers

Process results for glass ablation like, e.g. surface roughness, ablation depth and resulting ablation rate and ablation efficiency, can be strongly dependent on the number of layers by which the sample is ablated. Multiple processing strategies including the application of various numbers of layers can be found in literature, resulting in hardly comparable results. Ablation efficiencies for fused silica are obtained, e.g. by ablating “up to 400 layers” [23] or “up to 10 layers” [28]. To provide an indication of the comparability of the results presented in this paper with results from other research, the influence of the number of layers on the ablation efficiency and surface roughness are examined. Furthermore, some results presented in the following are obtained by ablation of N = 5 layers and are compared to the ablation of N = 10 layers. Therefore, the impact of the differing process strategy needs to be analyzed.

The ablation efficiency resulting from N-BK7 ablation in dependence of the number of layers for $N \leq 20$ is shown in **Fig 2** for 200 fs and 8 ps, exemplary for a fluence of F_0 = 10 J/cm². Because of the constant pulse overlap at the constant repetition rate of 100 kHz, the scanning speed is also kept constant. Thus, the course of efficiency as a function of the number of layers reflects the behavior of the ablation depth per layer.

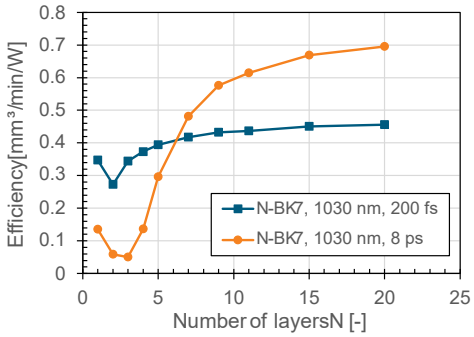

Fig 2 Ablation efficiency of N-BK7-ablation at 1030 nm in dependence of the number of layers for 200 fs and 8 ps, exemplary for a fluence of F_0 = 10 J/cm².

For both pulse durations, the efficiency drops after ablation of the first layer. Then, the efficiency for subsequent layers increases tending towards a parameter specific efficiency saturation threshold. A significantly different behavior is observed when comparing the ablation efficiency of the two pulse durations in the range of $N < 6$ and $N > 6$. In the first five layers, a lower efficiency of the ps-ablation compared to the fs-pulse duration is observed. For $N > 6$, the ps-efficiency exceeds the fs-efficiency due to a steep increase in the ps-efficiency. In general, the dependency of the ablation efficiency is more pronounced at 8 ps and the saturation regime is assumed to be reached beyond the upper limit of ϵ_{abl} = 0.70 mm³/min/W at N = 20 that is investigated here. The fs-ablation process is less dependent on the number of layers. Efficiencies of $0.27 \leq \epsilon_{abl} \leq 0.46$ mm³/min/W are obtained by the ablation with $N \leq 20$ and a saturation seems to be reached around N = 20 with ϵ_{abl} = 0.46 mm³/min/W.

The increasing efficiency with the number of ablation layers for both pulse durations is attributed to the incubation effect. Due to induced defects from prior pulse tracks, the absorption is increased resulting in a higher amount of deposited pulse energy contributing to the ablation. The initial drop after the first layer might be caused by debris from the first ablation layer which has to be removed. In the following ablation layers the previously mentioned reasons become dominant. The steeper increase in ablation efficiency for the 8 ps pulse duration is explained as follows:

I. Longer pulse durations lead to lower intensities at the same fluence and are dominated by Avalanche Ionization.

II. Avalanche ionization requires seed electrons which have to be excited by non-linear absorption mechanisms like multi-photon absorption.
III. Due to the flat curve of the energy along the time of one pulse, a reduced absorption threshold would lead to an earlier generation of free electron density. This would cause the Avalanche Ionization to start earlier as well, which leads to increased deposited pulse energy and increased ablation.
IV. In contrast, short pulses are dominated by multi-photon absorption where lower absorption thresholds are also beneficial. Nevertheless, their contribution is much smaller than the contribution from Avalanche Ionization for longer pulses.

The efficiency of P-SF69-ablation is less dependent on the applied number of layers than the ablation of N-BK7. Exemplary for two different parameter combinations, a DUV-ps-process at 8 ps and an IR-fs-process at 200 fs, the ablation efficiency in dependence of the number of layers is shown in **Fig 3**.

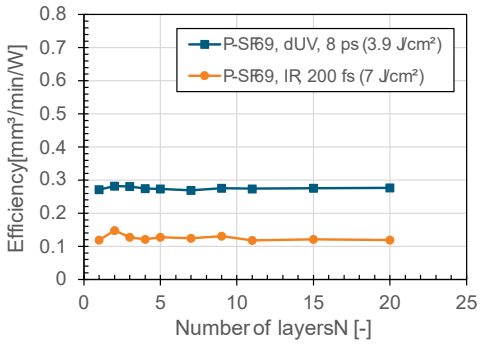

Fig 3 Ablation efficiency of P-SF69 ablation in dependence of the number of layers for the parameter settings λ_1 = 1030 nm, τ_1 = 200 fs, $F_{0,1}$ = 7 J/cm² and λ_2 = 266 nm, τ_2 = 8 ps, $F_{0,2}$ = 3.9 J/cm².

In the range of $N \leq 20$ the efficiency is almost independent from the number of layers, i.e. the ablation depth per layer is also constant. The reason for this behavior is investigated in the later course of this paper.

Overall, an ablation depth per layer, that is independent of the number of layers applied, is favorable regarding precise applications like optics manufacturing where form deviation is a crucial issue. If the ablation depth is dependent on the locally applied number of layers, the process needs to be conducted in the saturation regime. Thus, additional layers are required that do not directly contribute to the form generation of the component.

3.2 N-BK7 ablation at 1030 nm

The ablation results presented in this section are obtained with a wavelength of 1030 nm, a repetition rate of 100 kHz, a pulse and line overlap of 60 %, and the sample cavities are ablated by N = 10 layers. The ablation efficiency as a function of the fluence is depicted in **Fig 4** in dependence on the pulse duration in the range of τ_P = 0.2-8 ps.

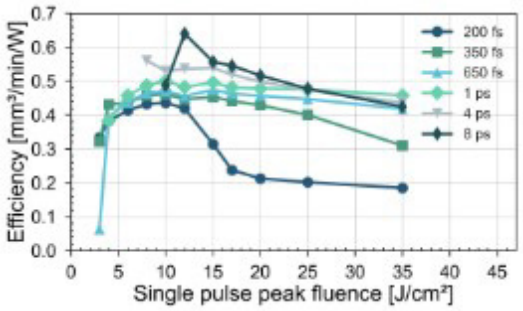

Fig 4 Ablation efficiency of N-BK7 ablation at 1030 nm as a function of the fluence in dependence on the pulse duration in the range of τ_P = 0.2-8 ps.

In general, the ablation efficiency increases with increasing fluence for pulse energies larger than the ablation threshold. A maximum efficiency is reached for a certain pulse duration dependent fluence, followed by a reduction of the efficiency with further increasing fluence. In consistency with results from literature [23], the well-known behavior of an increasing maximum ablation efficiency with increasing pulse duration for the ablation of transparent dielectrics is observed. The lowest maximum efficiency $\epsilon_{abl,max}$ = 0.44 mm³/min/W is obtained for τ_P = 200 fs at a fluence of about 10 J/cm². Following the max. efficiency, a significant drop of the efficiency is observed with increasing fluence, resulting in a low efficiency of ϵ_{abl} = 0.24 mm³/min/W already at F_0 = 17 J/cm² for this pulse duration. The window of a highly efficient ablation around the max. efficiency is broadened with increasing pulse duration up to about 1 ps and the decline in efficiency is spread over a wider range of fluences. The most efficient ablation, regarding the pulse durations investigated, of $\epsilon_{abl,max}$ = 0.64 mm³/min/W, is achieved with τ_P = 8 ps. But the process window between onset of ablation and decreasing efficiency is relatively narrow compared to shorter pulse durations.

For analysis of the underlying ablation characteristics and surface properties in the different ablation regimes, the ablation rate and the surface morphology are investigated. The ablation rate, which reflects the ablation depth per layer due to constant parameter settings, in dependence on the fluence under variation of the pulse duration is shown in **Fig 5**.

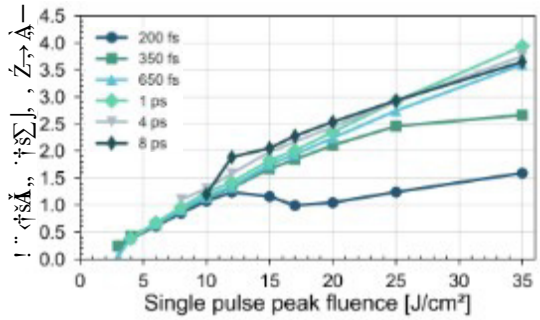

Fig 5 Ablation rate as a function of the fluence for the pulse durations τ_P = 0.2-8 ps for N-BK7 ablation at 1030 nm and 100 kHz.

An approximately linear relationship between ablation rate and fluence is observed for the higher pulse durations $\tau_P \geq$ 650 fs after the initial start of the ablation. The ablation rates of shorter pulse durations 200 and 350 fs exhibit a drop at a certain fluence. This drop is more pronounced for τ_P = 200 fs, where the ablation rate decreases from $\dot{V}_{abl}$ = 1.24

mm³/min at 12 J/cm² to $\dot{V}_{abl}$ = 1.0 mm³/min at 17 J/cm². With increasing pulse duration to τ_P = 350 fs, the drop of the ablation rate is shifted towards higher fluences and it only appears as a deviation from the linear relationship at about 25 J/cm². These drops are also observed in the ablation efficiency of these pulse durations (cf. **Fig 4**). Compared to longer pulse durations the ablation efficiency drops strongly at the mentioned fluences instead of a nearly constant behavior of longer pulse durations.

The increase of the ablation efficiency with increasing pulse duration can be explained by the change of the dominant absorption mechanism from multi-photon absorption for short pulses to Avalanche Ionization for longer pulses. The free electron density is mostly generated by multi-photon absorption for short pulse durations [19]. Due to the linear absorption behavior of the free electron density, a higher share of the pulse energy is deposited by means of Avalanche ionization leading to a more efficient transfer of anergy and thus to a higher ablation efficiency of the longer pulse durations.

Besides the ablation efficiency, the resulting surface quality is a critical parameter for high precision surface ablation processes. In **Fig 6**, the corresponding surface roughness after ablation with different pulse durations is shown as a function of the fluence.

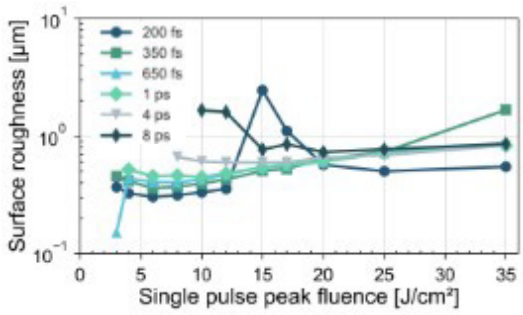

Fig 6 Surface roughness as a function of the fluence for the pulse durations τ_P = 0.2-8 ps after ablation of N-BK7 at 1030 nm and 100 kHz.

In general, surface roughness is increasing with increasing fluence for all pulse durations. The minimum roughness for each pulse duration is increasing with the pulse duration and is in the range of a few 100 µm. The minimum surface roughness of Sa = 0.3 µm is achieved with the shortest pulse duration of 200 fs at F_0 = 6 J/cm². One exception regarding the continuous increase of the roughness over the fluence is the 200 fs pulse duration. Corresponding to the drop in the ablation rate and the efficiency, which occur at F_0 = 15 J/cm² for 200 fs, a sharp maximum of the surface roughness is located at this point. Additionally, a second such increase of the roughness is indicated for 350 fs at F_0 = 35 J/cm², corresponding to the slight kink in the curves of the ablation rate and efficiency at the same point. Exemplary for the two extreme pulse durations of 200 fs and 8 ps, the underlying surface morphology is shown in **Fig 7**.

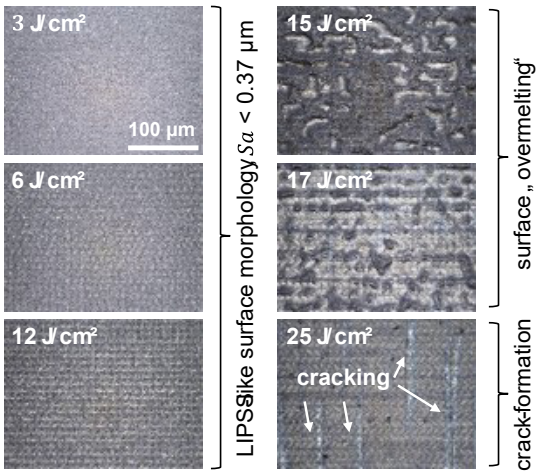

Fig 7 Surface morphology of N-BK7 ablation at 200 fs and 1030 nm, 100 kHz: LSM-measurements of exemplary fluences.

The fs-ablation is characterized by a relatively low surface roughness of Sa < 0.37 µm in the low fluence regime of $F_0 \leq$ 12 J/cm². The surface in this regime is homogeneously covered by LIPSS (cf. **Fig 19** (a)). With further increasing fluence in the range of about 15-17 J/cm², overmelting of the LIPSS structures is observed (cf. **Fig 8** (b)), resulting in the local maximum of the surface roughness, which is shown in **Fig 6**. Following, the surface roughness is reduced to a medium level about Sa = 0.5-0.6 µm by increasing the fluence to about > 17 J/cm². Apart from the evolution of the roughness, damage formation is increasingly observed with increasing fluence. Cracks are clearly visible in the LSM-images (**Fig 7**) at the highest fluence of F_0 = 25 J/cm². But crack-formation is beginning at lower fluences, as revealed by the SEM-images (cf. **Fig 8** (b)). The exact onset of crack-formation cannot be stated with certainty, but cracks are increasing with fluence. SEM-analysis using different detectors is indicating slight cracking also in the LIPSS-regime. In all cases of detected cracks, the progress of the cracks is linear and the orientation is perpendicular to the orientation of the scan vectors of the last layer. Linearly polarized laser radiation is used, but the influence of the scanning direction is assumed to be decisive. Different orientations of the scan vectors in the last layer are evaluated, and cracks are always orientated perpendicular to the scanning direction. Thus, the scanning direction is the dominant parameter for the direction of cracks.

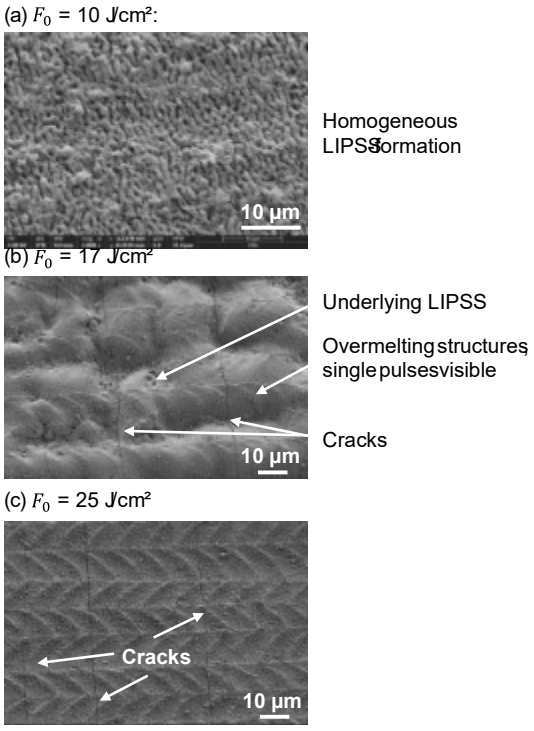

Fig 8 SEM-images of N-BK7 ablation at 200 fs, 100 kHz in the characteristic process-regimes: (a) LIPSS-structures, (b) high surface roughness due to overmelting structures, (c) severe crack-formation. In these images, the scanning direction and the polarization of the laser beam are horizontally oriented.

In the ps-process, the evolution of the surface roughness does not show a local peak but is rather constantly on a high level of about Sa = 0.7-0.9 µm. The surface morphology is illustrated by LSM-images in the range of 10-25 J/cm² in **Fig 9** and an exemplary SEM-image at F_0 = 25 J/cm² in **Fig 10**.

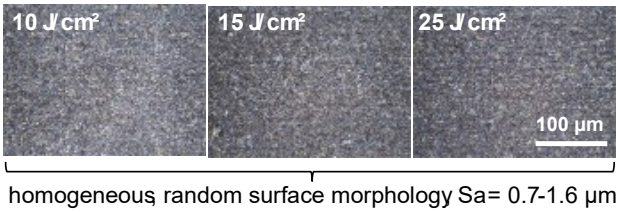

Fig 9 Surface modifications of N-BK7 processed with 8 ps and 1030 nm, 100 kHz: LSM-measurements of exemplary fluences.

The surface after ps-ablation is continuously covered by a rough structure with molten patterns indicating a thermal impact. The shape of single overlapping pulses like illustrated in **Fig 8** (c) for fs-ablation are not visible in the surfaces modified by ps-pulses.

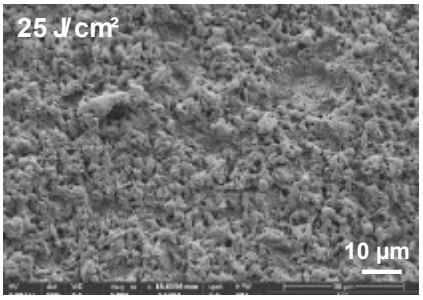

Fig 10 SEM-image of N-BK7 ablation at 8 ps, 100 kHz at F_0 = 25 J/cm².

Furthermore, crack-formation is not observed after ps-ablation. Only at the upper limit of fluences about 25 J/cm², first signs of small randomly orientated cracks are indicated by SEM-analysis. The damage formation in the fs-process is attributed to the multi-photon ionization process which is dominant in this regime. Besides energy deposition near the surface some energy is deposited in the volume under the ablation area due to the non-linear absorption. This energy leads to modification and stress below the surface resulting in cracks. In comparison, we assume that a major part of pulse energy is deposited near the surface during the ps-process due to the shift towards Avalanche Ionization as dominant absorption process. The initial free electrons on the surface absorb a major part of the subsequent photons preventing an absorption of these photons below the ablation volume.

3.3 Influence of the wavelength on the ablation behavior of N-BK7

In the following section, the ablation behavior at a wavelength of 1030 nm is compared to ablation conducted at DUV-wavelengths of 257 nm at 200 fs and 266 nm at 8 ps. For one setup, only small repetition rates could be applied. For comparability, all following results are conducted with a repetition rate of 10 kHz. In contrast to the ablation characteristics and surface morphologies presented in the previous **section 3.2**, it has to be noted that the overmelting structures, the corresponding drop in the ablation rate and the peak in the roughness are not present for the ablation at 10 kHz with N = 10 layers. Thus, these aspects can be attributed to heat accumulation due to shorter intervals between the pulses.

The influence of the pulse duration on the behavior of N-BK7 ablation is analyzed contrasting IR- and DUV-wavelenghts. Exemplary for a low and a high pulse duration, 200 fs and 8 ps are chosen for both wavelengths. In **Fig 11**, the ablation efficiency as a function of the fluence is presented for 200 fs and 8 ps, each for the IR- and DUV-wavelength.

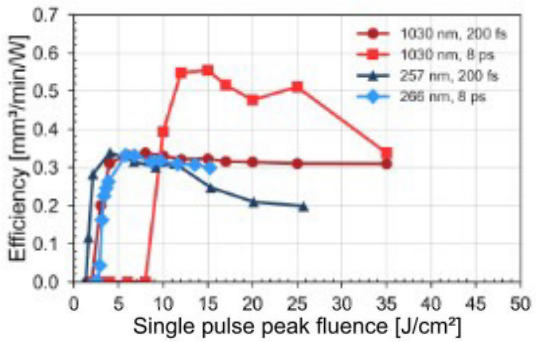

Fig 11 Efficiency of N-BK7 ablation contrasting the influence of the pulse duration of 200 fs vs. 8 ps for ablation with 1030 nm compared to 257-266 nm.

As already found in **section 3.2**, IR-ablation is strongly dependent on the pulse duration. Regarding the efficiency, the maximum ablation efficiency $\epsilon_{abl,max}$ = 0.55 mm³/min/W of ps-ablation is significantly higher than the maximum efficiency $\epsilon_{abl,max}$ = 0.34 mm³/min/W of fs-ablation. The difference to the results in **section 3.2** (cf. **Fig 4**) is attributed to the lower repetition rate and thus lower thermal impact which would cause higher ablation rates and efficiencies. The dependence of the ablation efficiency on the pulse duration for IR is already discussed above (cf. **section 3.2**).

In contrast, both fs- and ps-ablation with DUV-wavelength achieve a comparable max. ablation efficiency of $\epsilon_{abl,max} \approx$ 0.34 mm³/min/W. The independence of the efficiency of the pulse energy for DUV ablation is attributed to a shift from non-linear (for IR) to linear (for DUV) absorption mechanisms. The higher photon energy of DUV laser radiation is directly absorbed, overcoming the band gap of the N-BK7 glass and generating a free electron density.

As mentioned in the previous **section 3.2**, the surface roughness of IR-ablation is significantly higher for the ps-process compared to fs-ablation. The evolution of the surface roughness in dependence on the fluence is depicted in **Fig 12** for both wavelengths and pulse durations.

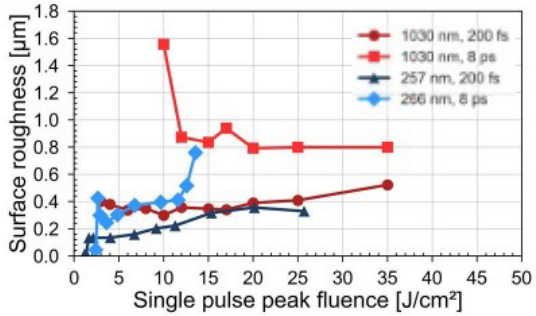

Fig 12 Surface roughness for N-BK7 ablation with 1030 nm and 257-266 nm, each at 200 fs and 8 ps.

Comparing the influence of the pulse duration within one wavelength, the fs-process is resulting in a lower surface roughness compared to the ps-process. Furthermore, lower surface roughness is achieved with DUV, at least when compared to IR within one pulse duration. At the point of max. efficiency of the DUV-fs-process at about F_0 = 4 J/cm², the surface roughness is Sa = 0.13 µm. The surface morphologies resulting from DUV-fs- and DUV-ps-ablation are illustrated by means of LSM-images in **Fig 13**.

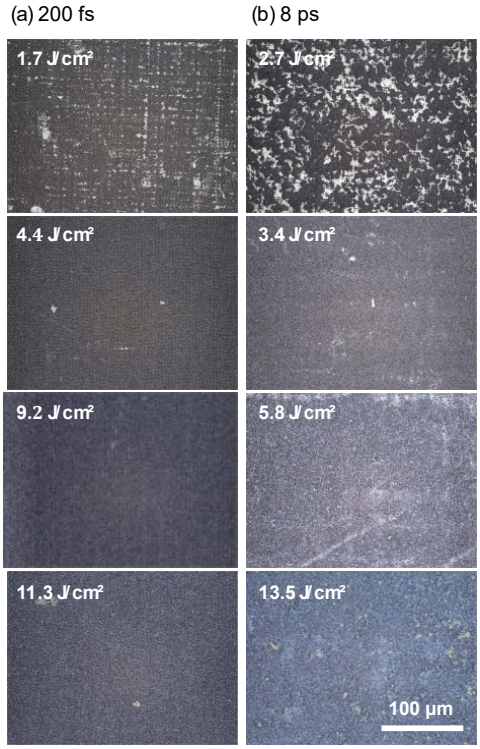

Fig 13 Surface morphology of N-BK7 ablation with (a) 200 fs at 257 nm and (b) 8 ps at 266 nm: LSM-measurements of exemplary fluences.

By only visual evaluation, no difference between the ablation mechanisms can be observed, but especially at the high fluences (bottom row in **Fig 13**) an increased surface roughness of ps-ablation is implied.

It should be noted at this point that three test series (IR-fs, IR-ps and DUV-ps) are conducted with N = 10 layers, but the DUV-fs-experiments are performed with N = 5 layers. As mentioned in section 3.1 (cf. **Fig 2**), the influence of the number of layers on the ablation depth is dependent on the laser parameters. To assess the influence of the number of layers for DUV-fs-ablation, the efficiency and the surface roughness are evaluated in dependence on the number of layers for N = 1-11 for two exemplary fluences. For 6.7 J/cm², around the point of max. efficiency, the efficiency is found to be independent from the number of layers for $N \geq 5$. For the higher fluence of 15.3 J/cm² investigated, the efficiency is slightly increasing between N = 5 and N = 10. Therefore, the max. efficiency shown in **Fig 11** is assumed to be comparable between the different processes, but the progression of the DUV-fs-graph could be slightly altered using N = 10 layers.

3.4 P-SF69 IR-ablation

All experiments regarding P-SF69 ablation are conducted with a constant repetition rate of 10 kHz, a line and pulse overlap of 60 % and N = 5 layers. Ablation of the dense-flint glass P-SF69 with reasonable ablation rates is very challenging. The ablation mechanism in IR is strongly dependent on the pulse duration. The huge difference in the efficiencies comparing the ablation with 200 fs and 8 ps is illustrated in **Fig 14** using a logarithmic scale of the y-axis.

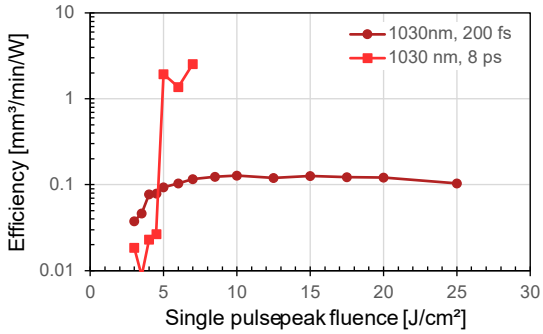

Fig 14 Efficiency of P-SF69-ablation with 1030 nm as a function of the fluence comparing the pulse durations 200 fs and 8 ps.

Compared to other glasses like N-BK7, the efficiency of fs-ablation of P-SF69 with a maximum of $\epsilon_{abl,max}$ = 0.13 mm³/min/W is very low. The ps-process in contrast, exhibits an extremely high ablation efficiency of about $\epsilon_{abl,max}$ > 2.5 mm³/min/W. Considering the surface roughness after ablation, a similar behavior in accordance with the ablation efficiency is observed, cf. **Fig 15**.

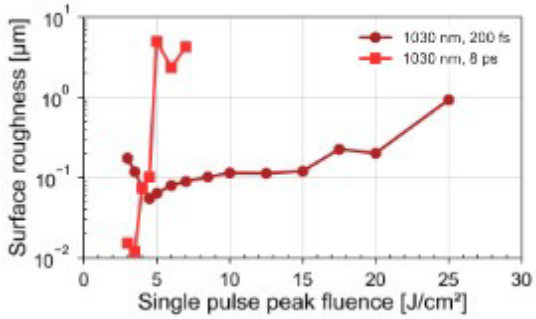

Fig 15 Surface roughness of P-SF69-ablation with 1030 nm at 200 fs and 8 ps.

Ablation with fs-pulses is resulting in a very low surface roughness of down to Sa = 55 nm at F_0 = 4.5 J/cm², which is unusually low for common glass ablation. The samples are nearly optically transparent after ablation. The difference between the fs- and the ps-process in contrast is huge, with a roughness of up to Sa = 5 µm after ps-ablation for fluences in the range of F_0 = 5-7 J/cm². Values of the surface roughness and the efficiency shown for IR-ps-ablation of P-SF69 are based on a coarse ablation, that is hardly controllable and should therefore be considered as a rough indication prone to variances.

The very small surface roughness after fs-ablation is resulting from a melt-based ablation process, indicating a thermal ablation mechanism. Due to a small ablation depth per layer, which is about Δz = 54 nm at F_0 = 3.0 J/cm² increasing to about Δz = 1 µm at F_0 = 17.5 J/cm², precision in depth is enabled but the ablation efficiency of up to 0.13 mm³/min/W is very low. A potential explanation might be given by the presence of heavy atoms like lead in the glass material. Further analysis needs to be conducted to evaluate if a stoichiometric ablation is performed or if the heavier elements will mostly remain heated on the glass surfaces leading to melt.

The surface morphology of fs-ablated P-SF69 is illustrated in **Fig 16**.

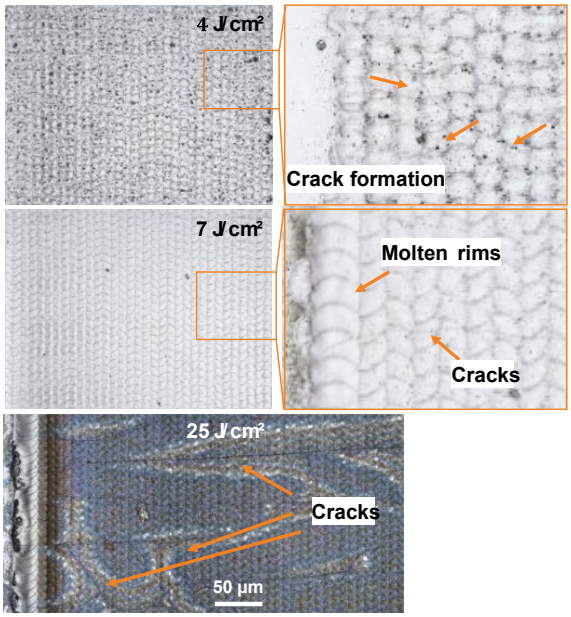

Fig 16 Surface morphology of P-SF69-ablation with 200 fs and 1030 nm at 10 kHz: LSM-measurements of exemplary fluences.

Already beginning at low fluences (cf, **Fig 16** (a), F_0 = 4 J/cm²), at the onset of ablation, crack-formation is observed. Crack-formation is intensified with increasing fluence resulting in a severely fragmentated surface at high fluences of about F_0 > 15 J/cm². Due to severe crack-formation, speed-up of the process by increasing the repetition rate is limited. The results presented are achieved with only a low repetition rate of 10 kHz. In combination with a low ablation depth per layer, the resulting process speed is < 0.1 mm³/min. Increasing the process speed and efficiency is possible by increasing the pulse duration to 8 ps, but the ablation mechanism is shifted to a coarse, uncontrolled photomechanical ablation. The ablation behavior at 8 ps is illustrated in **Fig 17**.

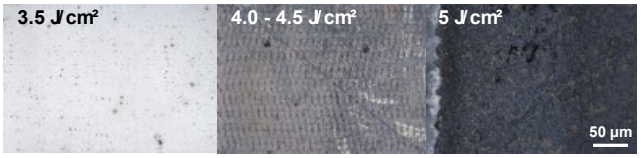

Fig 17 Surface morphology of P-SF69-ablation at 8 ps and 1030 nm with 10 kHz: LSM-measurements of (a) first modifications at F_0 = 3.5 J/cm², (b) small process window of fine ablation at F_0 = 4.0-4.5 J/cm², (c) coarse ablation for $F_0 \geq$ 5 J/cm².

At F_0 = 3.5 J/cm², first modifications on the surface are visible. Fine ablation with $Sa \approx$ 0.1 µm is detectable in the narrow range of about F_0 = 4.0-4.5 J/cm², but it is also accompanied by crack-formation. A small increase of the fluence to F_0 = 5.0 J/cm² leads to a highly rough surface with Sa = 5 µm, resulting from coarse, deep ablation. At this point, the ablation depth per layer amounts to Δz = 4.7 µm and the efficiency is ϵ_{abl} > 1.9 mm³/min/W. Regarding the two pulse durations investigated, IR-ablation is not well suitable for precise and efficient ablation. The very precise fs-ablation with very low surface roughness due to a thermal melt-based ablation is coming along with crack-formation starting

already at the beginning of the process window. A scaling of the process speed is limited by the repetition rate, as cracks are generated already at 10 kHz. The ps-ablation in contrast is a very coarse, deep, photo-mechanical ablation process, that is hardly controllable.

The notable difference between the ablation behavior of N-BK7 and P-SF69 is assumed to be based on the different chemical compositions of both glasses. The dense-flint glass P-SF69 exhibits a high density and is lead-containing. P-SF69 is a low-Tg-glass, i.e. having a low glass transition temperature, and therefore is also suitable for precision molding. The influence of the glass composition and the effect of heavy metal oxides on the ablation behavior need further investigation. Time-resolved in-situ analysis of the excitation during the ablation process could provide a more detailed understanding.

3.5 Influence of the wavelength on the ablation behavior of P-SF69

In the following, DUV-ablation of P-SF69 is investigated regarding the drawbacks of IR-ablation mentioned above. The ablation efficiency of DUV-ablation in comparison to IR-ablation is contrasted in **Fig 18** for 200 fs and 8 ps. The repetition rate is kept constant at 10 kHz and ablation is conducted with N = 5 layers.

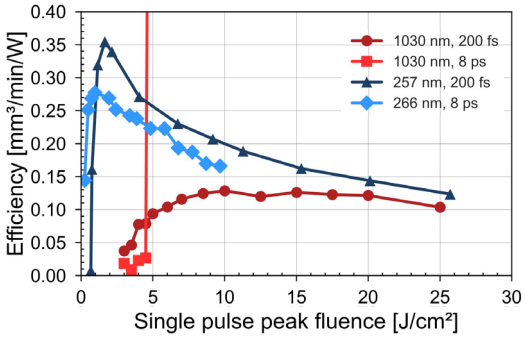

Fig 18 Efficiency of P-SF69 ablation contrasting the influence of the pulse duration (200 fs and 8 ps) on the ablation behavior using 1030 nm compared to 257-266 nm.

To keep the graphs legible, the scale of the y-axis is chosen neglecting the high efficiency beyond ϵ_{abl} > 2.5 mm³/min/W already at F_0 = 7 J/cm² of IR-ps-ablation (cf. **Fig 14**). Obviously, the efficiency of DUV-ablation is below the coarse ablation with IR at ps-pulse duration, but significantly higher than IR-fs-ablation. The maximum efficiencies are $\epsilon_{abl,max}$ = 0.35 mm³/min/W for fs-ablation at 257 nm and $\epsilon_{abl,max}$ = 0.28 mm³/min/W for ps-ablation at 266 nm. With this slightly higher efficiency of the fs-process compared to ps-ablation, the DUV-results of P-SF69-ablation are in the order of magnitude like DUV-ablation of N-BK7 with $\epsilon_{abl,max} \approx$ 0.34 mm³/min/W (cf. **section 3.3**). Furthermore, the two efficiency graphs of DUV-ablation of P-SF69 exhibit a similar progression indicating a similar ablation behavior.

The surface roughness as another indication for the ablation mechanism is analyzed. The influence of the pulse duration on the surface roughness of P-SF69-ablation is shown in **Fig 19**, contrasting IR- and DUV-wavelengths.

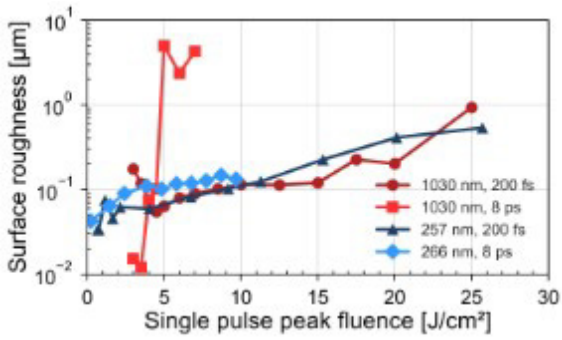

Fig 19 Surface roughness of P-SF69-ablation with 1030 nm and 257-266 nm, each at 200 fs and 8 ps.

A very low surface roughness is achieved for all processes except IR-ps-ablation. The huge difference between the roughness of fs- and ps-ablation in IR is explained by two different ablation mechanisms, namely thermal melt-based fs-ablation in contrast to a coarse photomechanical ablation with the ps-pulse duration. The low surface roughness during the ablation process is one explanation for the independence of the ablation depth from the number of ablation layers, as shown in section 3.1 (cf. **Fig 3**). Surface roughness and (sub-)surface defects are two factors influencing the absorptivity. Thus, the incubation effect is less pronounced for the ablation of P-SF69 ablation compared to N-BK7.

Considering DUV-ablation, the roughness is in the same order of magnitude as IR-fs-ablation with a very low roughness of Sa = 46 nm, achieved at the point of max. efficiency with DUV-fs-ablation. Thus, a highly efficient ablation is possible with DUV-fs ablation, simultaneously with a very low surface roughness. The ablation depth per layer at this point is about Δz = 260 nm.

The surface morphology after DUV-ablation with both pulse durations 200 fs and 8 ps is contrasted in **Fig 20**.

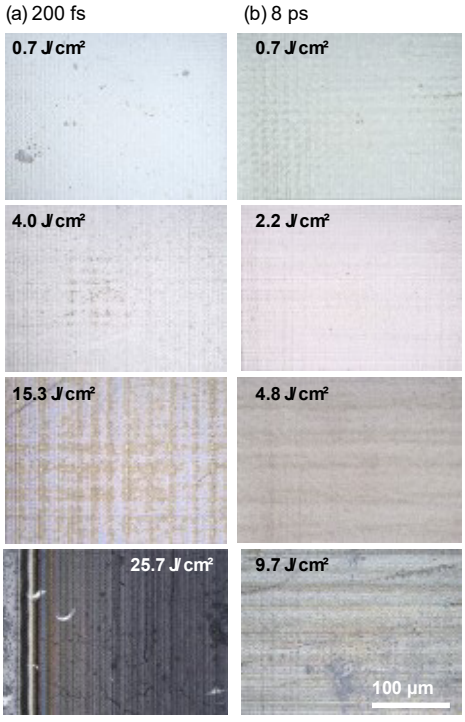

Fig 20 Surface morphology of P-SF69 ablation with (a) 200 fs at 257 nm and (b) 8 ps at 266 nm: LSM-measurements of exemplary fluences.

Visually evaluated, the surfaces of both processes show molten structures causing the comparable low surface roughness. Thus, the ablation mechanism is thermal and melt-based for both pulse durations and is assumed to be independent of the pulse duration in the USP-DUV-range. Crack-formation, that is clearly visible already for low fluences about 4 J/cm² on the fs-ablated surfaces in IR, is not obviously detectable after DUV-ablation with moderate fluences. Crack-formation is also observed for DUV-fs-ablation at very high fluences of about 25.7 J/cm² (cf. **Fig 20** (a), bottom).

4. Conclusion

The influence of the pulse duration in the fs-ps-range in two wavelength-regimes, namely IR at 1030 nm and DUV at 257-266 nm, on the ablation of optical glasses is investigated. The borosilicate-crown glass N-BK7 and the dense-flint glass P-SF69 are used representing two different types of optical glasses. Ablation and modification characteristics are evaluated based on ablation efficiency and surface roughness and are illustrated by means of the surface morphology. The applicability of different parameter combinations of pulse duration and wavelength regarding the requirements of precise optics manufacturing is investigated.

The ablation process at 1030 nm of the widely used optical glass N-BK7 is strongly dependent on the pulse duration. Ablation efficiency and ablation depth are significantly higher using ps-pulse durations compared to fs-pulses, accompanied by a higher surface roughness of ps-ablation. The maximum efficiency is $\epsilon_{abl,max}$ = 0.55 mm³/min/W for ps-ablation respectively $\epsilon_{abl,max}$ = 0.34 mm³/min/W for fs-ablation. This behavior is attributed to the avalanche ionization dominated absorption mechanism of the ps-process. The minimum surface roughness is about Sa = 0.30 µm for fs-ablation and Sa = 0.83 µm for ps-ablation showing a typical roughness and morphology of USP-modified glass surfaces.

DUV-ablation of N-BK7 in contrast is less dependent on the pulse duration than IR-ablation. An efficiency of about $\epsilon_{abl,max} \approx$ 0.34 mm³/min/W is obtained for both pulse durations 200 fs and 8 ps with comparable fluences. Thus, the ablation depth is independent from the pulse duration in DUV, which is attributed to the dominating linear absorption mechanisms for both pulse durations. The lowest surface roughness is achieved with DUV-fs-ablation. The DUV-ps-process is also resulting in a lower roughness compared to IR-ablation. The surface roughness of DUV-fs-ablation is continuously increasing with increasing fluence. An exemplary surface roughness is Sa = 0.13 µm at the point of max. efficiency at F_0 = 4 J/cm².

The ablation behavior of P-SF69 strongly differs from N-BK7 ablation and other commonly known glass materials like fused silica or soda-lime glass. IR-ablation with 200 fs shows a significant thermal impact resulting in a melt-based ablation with a very low surface roughness of down to Sa = 55 nm. Nevertheless, damage formation in form of cracks seeded under the surface due to energy deposition in the volume hinder the potential of this regime for optics manufacturing. IR-ps-ablation in contrast is an extremely coarse, uncontrolled deep ablation with ablation depth of several µm, resulting in a highly efficient ablation with ϵ_{abl} > 2.5 mm³/min/W, but also a highly rough surface of up to Sa = 5 µm. In contrast to fs-ablation, the coarse, deep ps-ablation is indicating a photomechanical ablation mechanism.

Using DUV-wavelengths, the mechanism of P-SF69-ablation is for both 200 fs and 8 ps pulse durations thermal and melt-based, resulting in smooth surfaces in both cases. A low surface roughness of Sa = 46 nm is achieved at the point of max. efficiency with F_0 = 1.65 J/cm² and 200 fs pulse duration. The maximum efficiencies are $\epsilon_{abl,max}$ = 0.35 mm³/min/W for fs-ablation at 257 nm and $\epsilon_{abl,max}$ = 0.28 mm³/min/W for ps-ablation at 266 nm, which is significantly higher than the low ablation efficiency of $\epsilon_{abl,max}$ = 0.13 mm³/min/W of IR-fs-ablation.

All results are obtained with industrial USP laser beam sources. On the one hand, an established USP IR-laser is used, on the other hand, DUV-wavelength is generated by commercially available fourth harmonic generation originating from an IR-source. To ensure comparability of the different laser parameter combinations and to investigate the fundamental mechanisms by avoiding accumulative processes, all experiments (except **section 3.2**) are conducted using a repetition rate of 10 kHz. It is important to note that 10 kHz is below typical industrial standards, where repetition rates of ≥100 kHz are generally employed. At higher repetition rates, factors such as heat accumulation, as well as plasma and particle shielding, become significant. These elements will be the focus of future research, which will build upon the insights gained from the current study, enabling a clear distinction between the influences of accumulative effects and the fundamental mechanisms that have been elucidated here.

A further topic currently under investigation is the effect of DUV-wavelengths on the scalability, i.e. particularly the formation of cracks. Regarding efficient optics manufacturing, targets of the ablation process are on the one hand a high process speed and high precision on the other hand. Hence, the goal is a possibly low ablation depth per layer to achieve precision in depth. Consequently, the scalable parameter for the ablation rate is the repetition rate, correlating with the scanning speed. Apparent crack-formation is observed for IR-fs-ablation of N-BK7 with 100 kHz. P-SF69 ablation is prone to crack-formation, which already occurs at 10 kHz and low fluences for IR-fs-ablation. Visually evaluated, Crack-formation with DUV at 10 kHz was only detectable at the upper limit of fluences applied and seems to be reduced especially for P-SF69 ablation. The applicability of higher repetition rates > 10 kHz with DUV-wavelengths is still under investigation.

Acknowledgments

We kindly acknowledge Light Conversion UAB for the possibility of conducting the DUV-fs-experiments with their Carbide laser with 4th harmonic module. The DUV-ps-experiments are enabled by the UV Center of Excellence, a cooperation between the Fraunhofer-Institute for Laser Technology and Coherent Corp.

References

[1] S. Schwarz, S. Rung, C. Esen, and R. Hellmann: Proc. SPIE, Vol. 11270, (2020) 112701E.
[2] M. Kahle, D. Conrad, S. Fricke, and L. Wilkens: J. Laser Micro Nanoeng., 17, (2022) 156.
[3] S. Schwarz, Rung Stefan, C. Esen, and R. Hellmann: J. Laser Micro Nanoeng., 13, (2018) 292.
[4] E. Kažukauskas, S. Butkus, V. Jukna, and D. Paipulas: Surf. Interfaces, 50, (2024) 104471.
[5] S. Schwarz, S. Rung, C. Esen, and R. Hellmann: Opt. Express, 26, (2018) 23287.
[6] S. Schwarz: J. Laser Micro Nanoeng., 12, (2017) 76.
[7] C. Weingarten, S. Heidrich, Y. Wu, and E. Willenborg: Proc. SPIE, Vol. 9633, (2015) 963303.
[8] M. Jung, T. Brunner, E. Willenborg, and C. Vedder: Opt. Express, 33, (2025) 15279.
[9] S. Heidrich, A. Richmann, P. Schmitz, E. Willenborg, K. Wissenbach, P. Loosen, and R. Poprawe: Opt. Lasers Eng., 59, (2014) 34.
[10] C. Weingarten, E. Uluz, A. Schmickler, K. Braun, E. Willenborg, A. Temmler, and S. Heidrich: Appl. Opt., 56, (2017) 777.
[11] B.-J. Meyer, G. Staupendahl, F. A. Müller, and S. Gräf: J. Laser Appl., 28, (2016) 012002-1.
[12] J. Ihlemann: Appl. Surf. Sci., 54, (1992) 193.
[13] J. Meinertz, A. Gödecke, L. J. Richter, and J. Ihlemann: Opt. Laser Technol., 152, (2022) 108148.
[14] C. Kalupka, D. Großmann, and M. Reininghaus: Appl. Phys. A, 123, (2017) 1.
[15] B. C. Stuart, M. D. Feit, S. Herman, A. M. Rubenchik, B. W. Shore, and M. D. Perry: Phys. Rev. B: Condens. Matter, 53, (1996) 1749.
[16] B. C. Stuart, M. D. Feit, A. M. Rubenchik, B. W. Shore, and M. D. Perry: Phys. Rev. Lett., 74, (1995) 2248.
[17] A. Kaiser, B. Rethfeld, M. Vicanek, and G. Simon: Phys. Rev. B: Condens. Matter, 61, (2000) 11437.
[18] A. Vogel, J. Noack, G. Hüttman, and G. Paltauf: Appl. Phys. B, 81, (2005) 1015.
[19] B. Rethfeld: Phys. Rev. B, 73, (2006) 035101-1.
[20] K. Cho, J. Choi, C. Ko, M. Kim, J. Lee, E. Eom, and S.-H. Cho: Int. J. Precis. Eng. Manuf., 25, (2024) 271.
[21] D. Stonyte, V. Jukna, D. Gailevičius, O. Balachninaite, P. Zakarauskas, and S. Juodkazis: Optica Open, (2025) 1.
[22] D. Stonyte, V. Jukna, and D. Paipulas: J. Laser Micro Nanoeng., 17, (2022) 121.
[23] N. Hodgson, A. Steinkopff, S. Heming, H. Allegre, H. Haloui, T. Lee, M. Laha, and J. VanNunen: Proc. SPIE, Vol. 11673, (2021) 1167308.
[24] G. Raciukaitis: IEEE J. Select. Topics Quantum Electron., 27, (2021) 1.
[25] J. Bliedtner, C. Schindler, M. Seiler, S. Wächter, M. Friedrich, and J. Giesecke: Laser Tech. J., 13, (2016) 46.
[26] SCHOTT, "Downloads for Optical Glass", https://www.schott.com/en-gb/products/optical-glass-p1000267/downloads (Accessed 4 July 2025), (2023).
[27] J. M. Liu: Opt. Lett., 7, (1982) 196.
[28] Y. Yang, K. Bischoff, D. Mücke, C. Esen, and R. Hellmann: J. Laser Appl., 36, (2024) 012019-1.

(Received: July 12, 2025, Accepted: December 21, 2025)